

# OOVDet: Low-Density Prior Learning for Zero-Shot Out-of-Vocabulary Object Detection

Su Binyi<sup>1</sup> Huang Chenghao<sup>1</sup> Chen Haiyong<sup>1</sup>

## Abstract

Zero-shot out-of-vocabulary detection (ZS-OOVD) aims to accurately recognize objects of in-vocabulary (IV) categories provided at zero-shot inference, while simultaneously rejecting undefined ones (out-of-vocabulary, OOV) that lack corresponding category prompts. However, previous methods are prone to overfitting the IV classes, leading to the OOV or undefined classes being misclassified as IV ones with a high confidence score. To address this issue, this paper proposes a zero-shot OOV detector (OOVDet), a novel framework that effectively detects predefined classes while reliably rejecting undefined ones in zero-shot scenes. Specifically, due to the model's lack of prior knowledge about the distribution of OOV data, we synthesize region-level OOV prompts by sampling from the low-likelihood regions of the class-conditional Gaussian distributions in the hidden space, motivated by the assumption that unknown semantics are more likely to emerge in low-density areas of the latent space. For OOV images, we further propose a Dirichlet-based gradient attribution mechanism to mine pseudo-OOV image samples, where the attribution gradients are interpreted as Dirichlet evidence to estimate prediction uncertainty, and samples with high uncertainty are selected as pseudo-OOV images. Building on these synthesized OOV prompts and pseudo-OOV images, we construct the OOV decision boundary through a low-density prior constraint, which regularizes the optimization of OOV classes using Gaussian kernel density estimation in accordance with the above assumption. Experimental results show that our method significantly improves the OOV detection performance in zero-shot scenes. The code is available at <https://github.com/binyisu/OOV-detector>.

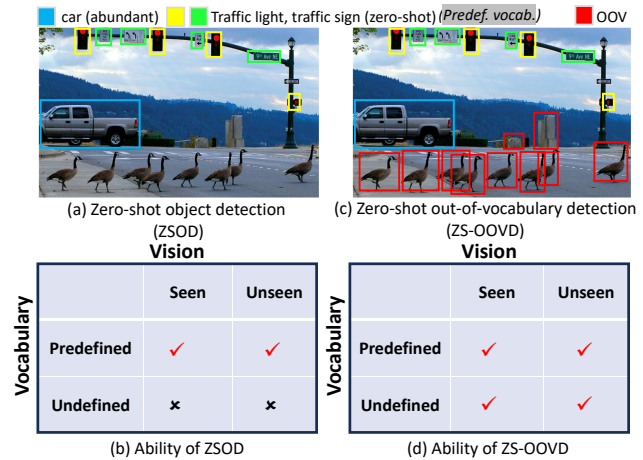


Figure 1. The zero-shot object detection (ZSOD) task vs the zero-shot out-of-vocabulary detection (ZS-OOVD) task.

## 1. Introduction

Zero-shot object detection (ZSOD) (Bansal et al., 2018; Cheng et al., 2024) has garnered significant attention for its ability to detect unseen categories at inference. The integration of vision-language models (Radford et al., 2021) and prompt learning (Zhou et al., 2022b) has advanced ZSOD (Qutub et al., 2024; Guo et al., 2025) and open-vocabulary object detection (OVOD) (Minderer et al., 2022; 2023). However, in real-world scenarios, numerous objects fall outside the predefined vocabulary, as illustrated in Fig. 1 (c). For instance, applying a vocabulary such as ['car', 'traffic light', 'traffic sign'] to the image in Fig. 1 (c) may lead to the misdetection or omission of objects not covered by the predefined categories. This highlights a critical challenge: how can a zero-shot model accurately identify objects within the predefined vocabulary while reliably rejecting objects from undefined categories?

In practice, this problem is more challenging than conventional ZSOD. As illustrated in Fig. 1(d), we define a new task, termed zero-shot out-of-vocabulary object detection (ZS-OOVD), which requires rejecting semantic concepts beyond a predefined vocabulary. In contrast to ZSOD's visual-centric treatment of unknowns, ZS-OOVD adopts a language-centric perspective with an explicit focus on vocabulary boundaries. Despite its practical importance, this problem has not been explicitly formulated or systematically studied, as existing ZSOD approaches focus on detecting

<sup>1</sup>School of Artificial Intelligence and Data Science, Hebei University of Technology, Tianjin, China. Correspondence to: Su Binyi <leo.subinyi@gmali.com>.

unseen classes within a fixed vocabulary while largely ignoring continuously emerging out-of-vocabulary objects in open-world scenarios. This gap highlights the necessity of investigating ZS-OOVD, particularly for safety-critical applications. Motivated by this gap, we take a first step toward defining the ZS-OOVD task, establishing a benchmark, and proposing an effective framework, termed OOVDet, which achieves reliable OOV detection while maintaining high accuracy on predefined categories.

Specifically, existing models lack prior knowledge of OOV data distributions, including OOV prompts and images. Due to the absence of these categories in training, models lack both semantic and visual priors, resulting in weak decision boundaries and unreliable predictions for OOV objects. To mitigate these issues, we first introduce a region-level Out-of-vocabulary Prompt Synthesis (OPS) mechanism that samples from the low-likelihood regions of IV class-conditional Gaussian distributions in the hidden space, motivated by the assumption that OOV semantics are more likely to emerge in low-density areas of the latent manifold. For the IV data, we first provide predefined question-answer (Q&A) pairs and templates that incorporate category names, for example: **Q:** [CLS] What object can be seen in the region? **A:** [CLS] The object is <cls>. We then guide ChatGPT through multiple rounds of prompt standardization to construct an IV class-specific prompt library, sampled during data preparation. These prompts are encoded by a text encoder to obtain embeddings, followed by the addition of masked Gaussian noise to form an IV class-conditional Gaussian distribution. This distribution is then used to synthesize OOV prompt embeddings in the latent space. Additionally, owing to the absence of training images for OOV classes, we select high-uncertainty samples from region proposals and treat them as pseudo-OOVs for optimization. Unlike prior energy-based mining methods (Joseph et al., 2021; Su et al., 2024), we propose a Dirichlet-based Gradient Attribution (DGA) approach that models attribution gradients as Dirichlet evidence to estimate predictive uncertainty and mine high-uncertainty samples as pseudo-OOV instances.

In particular, given the observation that in-vocabulary objects cluster in high-density regions while out-of-vocabulary objects reside in low-density areas (Han et al., 2022; Ren et al., 2018), proper separation of these regions is essential for reliable OOV decision boundaries. Prior methods (Han et al., 2022) expand low-density regions via contrastive learning but do not explicitly enforce density separation. In contrast, we adopt a density estimation strategy, using Gaussian kernel density estimation to push pseudo-OOV samples into low-density regions and away from dense IV clusters. Specifically, we propose a Low-density Prior Constraint (LPC) to regularize OOV optimization and promote discriminative IV-OOV decision boundaries.

In summary, the contribution of this paper is three-fold:

- To the best of our knowledge, this is the first work

to confront the challenging ZS-OOVD task, which achieves effective OOV rejection without degrading performance on the predefined closed-set vocabulary.

- We propose a novel OOV detector, termed OOVDet, which integrates three well-designed modules-OPS, DGA, and LPC-to enable robust and reliable IV-OOV discrimination.
- We introduce a new ZS-OOVD benchmark. Compared to previous methods, our approach consistently achieves substantially higher recall for OOV classes, providing 4.77 - 8.70% improvements across different settings of OOV datasets.

## 2. Related Works

### 2.1. Out-of-Vocabulary Detection

Out-of-vocabulary (OOV) detection was originally studied in speech recognition (Young, 1994) and has recently attracted attention in computer vision with the emergence of vision-language models and prompt learning. However, OOV detection in zero-shot settings remains largely under-explored. Unlike conventional zero-shot or open-vocabulary detection (Zhong et al., 2022), zero-shot OOV detection lacks both visual exemplars and reliable linguistic priors for OOV categories, making accurate recognition and localization particularly challenging. Recent studies have attempted to mitigate unknown modeling by introducing pseudo-sample generation or proxy supervision (Wu et al., 2025; Su et al., 2023). Inspired by this line of work, we propose an OOV prompt synthesis and pseudo-OOV image mining framework that compensates for the absence of real OOV supervision, alleviates prior deficiency.

### 2.2. Zero-Shot and Open-Vocabulary Object Detection

Zero-shot and open-vocabulary object detection leverage large-scale image-text pretraining to recognize unseen categories via visual-textual alignment (Bansal et al., 2018; Zhong et al., 2022; Minderer et al., 2022). While effective for unseen but predefined classes, these methods are restricted to IV prediction and often misclassify undefined OOV objects into semantically similar IV categories with high confidence. From a representation perspective, supervised learning induces compact, high-density IV clusters, whereas OOV samples tend to occupy low-density regions between clusters. Density-aware methods such as OpenDet (Han et al., 2022) and AKCR (Sarkar et al., 2024) exploit this property via feature compactness or semantic alignment, but depend on unknown-class supervision or are unsuitable for zero-shot OOV detection, leading to limited OOV rejection. To overcome this limitation, we propose a low-density prior learning method that constrains pseudo-OOV priors in low-density regions using Gaussian kernel density estimation, thereby constructing discriminative IV-OOV boundaries without real OOV supervision, and improving OOV detection performance in a zero-shot setting.

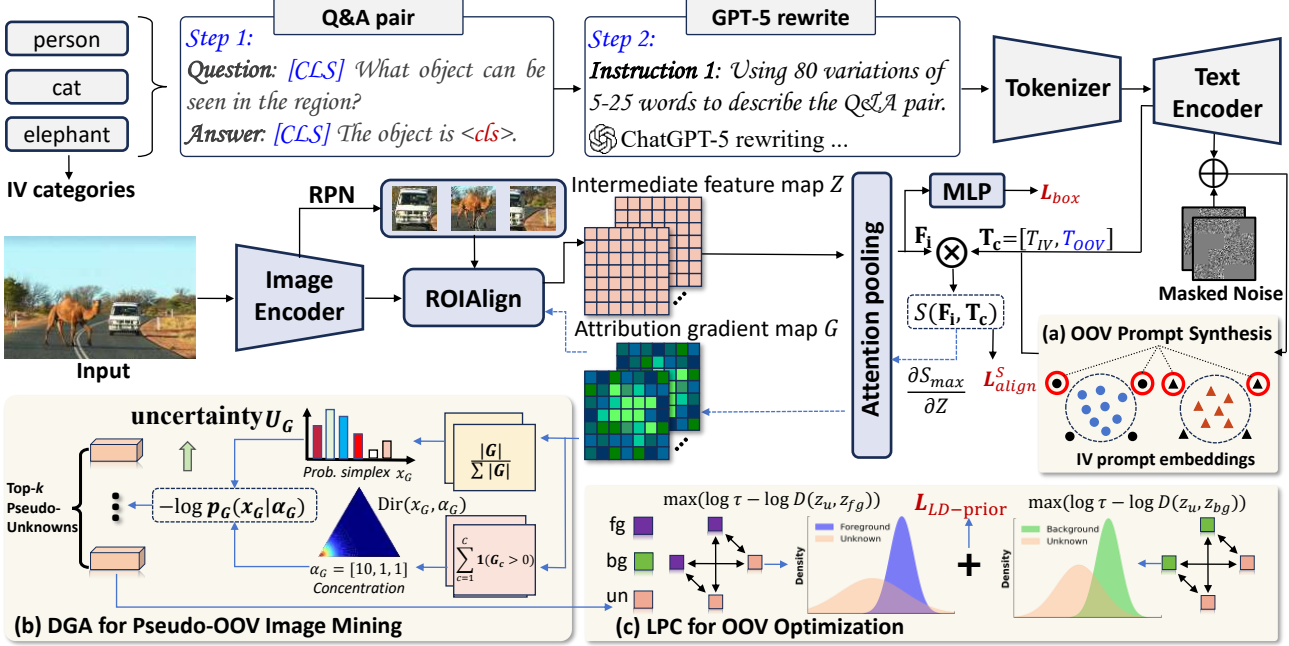


Figure 2. The framework of our OOVDet for the challenging zero-shot out-of-vocabulary object detection task. OOVDet is a simple two-stage detector with (a) a novel Out-of-vocabulary Prompt Synthesis (OPS), (b) a novel Dirichlet-based Gradient Attribution (DGA) for pseudo-unknowns mining and (c) a novel Low-density Prior Constraint (LPC) for OOV optimization.

### 3. Method

We define the ZS-OOVD problem setup with reference to ZSOD task (Bansal et al., 2018) and OOV detection task (Young, 1994). As illustrated in Fig. 3, given an object detection dataset  $D = (x, y)$ , where  $x \in \mathbf{X}$  denotes an input image and  $y = \{(c_i, \hat{b}_i)\}_{i=1}^I$  represents objects with their class label  $c_i$  and bounding box  $\hat{b}_i$ , the dataset is divided into a training set  $D_{tr}$  and a testing set  $D_{te}$ . The training set  $D_{tr}$  contains  $S$  seen classes denoted as  $C_{Seen}$ , with predefined vocabularies. In practice, the testing set  $D_{te}$  includes the category set  $C_T = C_{Seen} \cup C_{Unseen} \cup C_{OOV}$ , where  $C_{Unseen}$  denotes  $Z$  predefined unseen classes, and  $C_{OOV}$  represents undefined classes that are entirely unknown to the model. By definition,  $(C_{Seen} \cup C_{Unseen}) \cap C_{OOV} = \emptyset$ . Given the unbounded number of unknown categories in open-world settings, we consolidate them into a single “OOV” class. Accordingly, the objective is to train a detector on  $D_{tr}$  that jointly recognizes  $S$  seen classes,  $Z$  unseen classes, and one OOV class under an open-set assumption. Here we let  $K = S + Z$ . Accordingly, the final scores are predicted as: scores = [seen<sub>1</sub>, ..., seen<sub>S</sub>, unseen<sub>1</sub>, ..., unseen<sub>Z</sub>, OOV].

#### 3.1. Baseline Setup

We setup the baseline with RegionClip (Zhong et al., 2022), which consists of a image encoder, a text encoder, a separately trained region proposal network (RPN), and an R-CNN. Conventional prompt learning aligns each proposal feature  $\mathbf{F}_i$  with its corresponding class prompt  $\mathbf{T}_c$  by com-

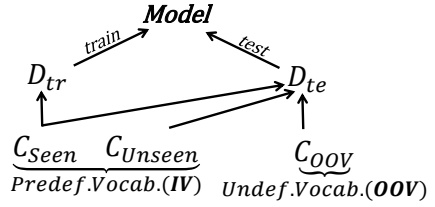


Figure 3. Problem Setup of ZS-OOVD.

puting their cosine similarity  $S(\mathbf{F}_i, \mathbf{T}_c)$ , which serves as the semantic alignment objective for category optimization:

$$L_{align}^S = -\frac{1}{N} \sum_{i=1}^N \sum_{j=1}^{K+2} y_{ij} \log \frac{\exp(S(\mathbf{F}_i, \mathbf{T}_j)/\tau)}{\sum_{c=1}^K \exp(S(\mathbf{F}_i, \mathbf{T}_c)/\tau)}, \quad (1)$$

where  $S(\cdot, \cdot)$  represents the cosine similarity and  $\tau$  denotes the temperature parameter,  $y_{ij}$  is an indicator (0 or 1) of sample  $i$  belonging to category  $j$  in the ground truth label. Compared with the RegionClip, we propose an Out-of-vocabulary Prompt Synthesis (OPS) for text embedding representation of undefined vocabulary, a Dirichlet-based Gradient Attribution (DGA) module for pseudo-OOV image mining, a Low-density Prior Constraint (LPC) loss for OOV optimization, as shown in Fig. 2.

For IV categories, ChatGPT-5 is used to rewrite predefined Q&A pairs, generating multiple prompt variants to form a class-specific prompt library, where the `<cls>` token is replaced with the corresponding category label. These prompts are fed into the text encoder, resulting in a bag-of-words tensor  $\mathbf{B}$ . After averaging by category, we obtain

the final IV prompt representation  $\mathbf{T}_{IV}$ . For OOV categories, random masked Gaussian noise is added to each IV prompt embedding in  $\mathbf{B}$ , forming a class-conditional Gaussian distribution. Then, this distribution is used to synthesize the virtual OOV prompt representation  $\mathbf{T}_{OOV}$  within the low-likelihood region of the IV class-conditional Gaussian distribution in the latent space. The prompt embedding of all categories is given as  $\mathbf{T}_c = \{\mathbf{T}_{IV}, \mathbf{T}_{OOV}\}$ .

### 3.2. Out-Of-Vocabulary Prompt Synthesis

Prior methods (Wu et al., 2025; Su et al., 2024) focus on visual feature mining and ignore textual OOV prompts, limiting explicit modeling of IV-OOV distributional gaps. To address this, we separate IV and OOV prompts in latent space and generate region-level pseudo-OOV prompts via Gaussian outlier sampling from low-likelihood regions of class-conditional IV Gaussians, enabling contrastive text–image alignment across IV and OOV. Assuming sufficient data, IV prompt embeddings from the text encoder are modeled as class-conditional multivariate Gaussian distributions:

$$p_\theta(\vec{T} \mid \vec{y} = i) = \mathcal{N}(\vec{\mu}_i, \hat{\sigma}), \quad (2)$$

where  $\theta$  denotes the parameters of the text encoder  $f_\theta$ ,  $\vec{y}$  is the ground-truth label,  $\vec{\mu}_i$  is the empirical Gaussian mean of the  $i$ -th IV class prompts embedding, and  $i \in \{1, \dots, K\}$  with  $K$  being the number of IV classes (seen + predefined unseen). The Gaussian distribution is defined as:

$$\mathcal{N}(\vec{\mu}_i, \hat{\sigma}) = \frac{1}{\sqrt{2\pi\hat{\sigma}^2}} \exp\left(-\frac{(\vec{T} - \vec{\mu}_i)^2}{2\hat{\sigma}^2}\right),$$

where  $\hat{\sigma}$  is the tied covariance matrix across all IV classes.

The empirical mean of the  $i$ -th IV class prompts embedding is computed as:

$$\vec{\mu}_i = \frac{1}{|\mathcal{Q}_T|} \sum_{j=1}^{|\mathcal{Q}_T|} \vec{T}_{i,j}, \quad (3)$$

where  $|\mathcal{Q}_T|$  is the size of the prompts queue  $\mathcal{Q}_T \in \mathbb{R}^{K \times |\mathcal{Q}_T|}$ . The tied covariance matrix is estimated as:

$$\hat{\sigma} = \frac{1}{K|\mathcal{Q}_T|} \sum_{i=1}^K \sum_{j=1}^{|\mathcal{Q}_T|} (\vec{T}_{i,j} + \alpha \mathbf{m} \odot \vec{\epsilon} - \vec{\mu}_i) \cdot (\vec{T}_{i,j} + \alpha \mathbf{m} \odot \vec{\epsilon} - \vec{\mu}_i)^T + \beta \mathbf{E}, \quad (4)$$

where  $\mathbf{m} \sim \text{Bernoulli}(\cdot)$  is a random mask vector,  $\vec{\epsilon}$  is a learnable noise matrix following a Gaussian distribution,  $\mathbf{E}$  is the identity matrix, and  $\alpha, \beta$  are hyperparameters. Here, the masked noise stabilizes  $\hat{\sigma}$  by preventing degeneration and ensuring a well-conditioned inverse.

Using these estimated Gaussian parameters, the prompt synthesis module samples virtual OOV prompts from the

low-likelihood regions of each IV class distribution:

$$\vec{v}_i \in \Psi(\vec{T}, \vec{\mu}_i, \hat{\sigma}), \quad (5)$$

where  $\Psi$  denotes the class-conditional Gaussian distribution probability density. The joint probability across all IV classes is:

$$\Psi(\vec{T}, \vec{\mu}_1, \dots, \vec{\mu}_K, \hat{\sigma}) = \prod_{i=1}^K \Psi(\vec{T}, \vec{\mu}_i, \hat{\sigma}). \quad (6)$$

For each  $\Psi(\vec{T}, \vec{\mu}_i, \hat{\sigma})$ , the low-likelihood region is defined as:

$$\begin{aligned} \Psi(\vec{T}, \vec{\mu}_i, \hat{\sigma}) = & \left\{ \vec{v}_i \sim \mathcal{N}(\vec{\mu}_i, \hat{\sigma}) \mid \frac{1}{(2\pi)^{d/2} |\hat{\sigma}|^{1/2}} \cdot \right. \\ & \left. \exp\left[-\frac{1}{2}(\vec{v}_i - \vec{\mu}_i)^T \hat{\sigma}^{-1}(\vec{v}_i - \vec{\mu}_i)\right] < \varepsilon \right\}, \end{aligned} \quad (7)$$

where  $\vec{v}_i$  is a virtual OOV prompt representation sampled from the  $i$ -th IV class,  $d$  is the embedding dimension, and  $\varepsilon$  is a threshold controlling the low-likelihood region. Since the exponent term in Eq. (7),  $D_i(\vec{v}_i) = -\frac{1}{2}(\vec{v}_i - \vec{\mu}_i)^\top \hat{\sigma}^{-1}(\vec{v}_i - \vec{\mu}_i)$  is proportional to the Mahalanobis distance, samples with larger distances lie in lower-likelihood regions of the IV distribution. In practice, we rank all perturbed candidates by their Mahalanobis distance and take the lowest-likelihood sample as the synthesized OOV prompt embedding  $\mathbf{T}_{OOV}$ .

### 3.3. Dirichlet-based Gradient Attribution for Pseudo-OOV image Mining

The lack of real OOV images during training hinders reliable OOV boundary construction, and prior methods (Han et al., 2022; Su et al., 2023) mainly mine high-uncertainty pseudo-unknown samples using logit-based metrics which may not fully capture deeper uncertainty. Motivated by attribution-based interpretability methods (Simonyan et al., 2013; Selvaraju et al., 2017), we model intermediate-layer gradients using a generalized Dirichlet distribution. As illustrated in Fig. 2(b), the attribution gradient  $G$  is defined as the partial derivative of the classification similarity  $S$  with respect to the layer parameters  $Z$ . Analogous to Grad-CAM (Selvaraju et al., 2017), we select the three lowest-density foreground proposals under the Dirichlet model as pseudo-OOV candidates. In Dirichlet distribution, the probability density of the gradient map can be expressed as:

$$\begin{aligned} \log p_G(x_G^n \mid \alpha_G^n) = & \underbrace{\sum_{c=1}^C (\alpha_G^{n,c} - 1) \log x_G^{n,c}}_{\text{Data term}} \\ & - \underbrace{\left( \sum_{c=1}^C \log \Gamma(\alpha_G^{n,c}) - \log \Gamma\left(\sum_{c=1}^C \alpha_G^{n,c}\right) \right)}_{\text{Normalization term}}, \end{aligned} \quad (8)$$

where  $\Gamma$  is the Gamma function used to calculate the normalization coefficients of the Dirichlet distribution,  $n = 1, 2, \dots, N$  indexes each proposal.  $x_G$  and  $\alpha_G$  denote the probability simplex and the concentration in Dirichlet function, respectively.

Since each proposal yields  $C$  gradient maps and the attribution gradients are assumed to follow a generalized Dirichlet distribution ( $x_G \sim \text{Dir}(x_G, \alpha_G)$ ), jointly estimating  $\alpha_G$  is computationally expensive. We therefore approximate  $\alpha_G$  using the frequency of positive gradients across channels, preserving essential distributional cues while reducing computation. The probability simplex  $x_G$  and the concentration  $\alpha_G$  can be jointly expressed by:

$$\begin{aligned} x_G^{n,c} &= \left| \frac{\partial S_{max}^n}{\partial Z_{n,c}} \right| \Big/ \sum_{c=1}^C \left| \frac{\partial S_{max}^n}{\partial Z_{n,c}} \right|, \\ \alpha_G^{n,c} &= \sum_{w=1}^W \sum_{h=1}^H \mathbf{1} \left( \frac{\partial S_{max}^n}{\partial Z_{n,c,w,h}} > 0 \right), \end{aligned} \quad (9)$$

where  $S_{max}$  denotes the maximum classification similarity. As shown in Fig. 2 (b), we quantify the uncertainty  $\mathcal{U}$  of each proposal using the negative log-probability density of the gradient distribution, and leverage the resulting high-uncertainty pseudo-OOV instances to enhance the OOV-class modeling:

$$\mathcal{U} = -\log(p_G(x_G \mid \alpha_G)). \quad (10)$$

Furthermore, since background proposals often overwhelm the mini-batch, we adopt balanced sampling with equal numbers of foreground and background proposals, which improves the model’s ability to recall OOV objects appearing in the background class.

### 3.4. Low-Density Prior Constraint for OOV Optimization

In supervised learning, IV-class samples are tightly aligned and form compact, high-density clusters in the embedding space. OOV samples, lacking such alignment, naturally reside in the low-density regions between these clusters. This distributional gap motivates our Low-Density Prior Constraint, which explicitly uses these low-density regions as priors to guide OOV optimization. To learn pseudo-OOV characteristics, we introduce a placeholder outside the existing vocabulary to represent OOV classes and leverage the low-density prior to model IV-OOV relations. Given pseudo-OOV samples  $z_u \in \mathbb{R}^{A \times d}$  and an IV feature bank  $z_{IV} = \{z_1, \dots, z_N\} \in \mathbb{R}^{N \times d}$ , we estimate the density between each OOV sample and  $z_{IV}$  using a Gaussian kernel:

$$\hat{p}(z_u^{(j)}) = \frac{1}{N} \sum_{i=1}^N \frac{1}{(2\pi h^2)^{d/2}} \exp \left( -\frac{\|z_u^{(j)} - z_i\|^2}{2h^2} \right), \quad (11)$$

where  $A$  is the number of pseudo-OOV samples,  $h$  is the kernel bandwidth, and  $d$  is the feature dimension. For each pseudo-OOV sample, we enforce a low-density prior on pseudo-OOVs via their log-density and apply it separately to foreground and background proposals.

**Foreground pseudo-OOVs.** The low-density constraint for foreground pseudo-OOV proposal features is defined as:

$$\mathcal{L}_{LD}^{fg} = \frac{1}{B_{fg}} \sum_{j=1}^{B_{fg}} \underbrace{s_j^{fg} (1 - s_j^{fg})^\alpha}_{t_j^{fg}} \cdot \max(\log \hat{p}(z_{u,fg}^{(j)}) - \log \hat{\tau}, 0), \quad (12)$$

where  $z_{u,fg}^{(j)}$  denotes the  $j$ -th foreground pseudo-OOV proposal feature,  $s_j^{fg}$  is the ground-truth probability for the  $j$ -th foreground sample, and  $B_{fg}$  is the number of foreground pseudo-OOV samples.  $t_j^{fg}$  is the corresponding weighting factor.  $\hat{\tau}$  denotes the density threshold.

**Background pseudo-OOVs.** Refer to the definitions of all parameters in the low-density constraint for foreground pseudo-OOV proposal features (Section “Foreground pseudo-OOVs”). The low-density constraint for background pseudo-OOV samples is given by:

$$\mathcal{L}_{LD}^{bg} = \frac{1}{B_{bg}} \sum_{j=1}^{B_{bg}} \underbrace{s_j^{bg} (1 - s_j^{bg})^\alpha}_{t_j^{bg}} \cdot \max(\log \hat{p}(z_{u,bg}^{(j)}) - \log \hat{\tau}, 0). \quad (13)$$

**Total low-density prior constraint.** The overall loss combining foreground and background components is:

$$\mathcal{L}_{LD-prior} = \mathcal{L}_{LD}^{fg} + \mathcal{L}_{LD}^{bg}, \quad (14)$$

where  $\mathcal{L}_{LD}^{fg}$  and  $\mathcal{L}_{LD}^{bg}$  denote the low-density losses for foreground and background pseudo-OOV samples, respectively. This formulation penalizes pseudo-OOVs only in high-density IV regions, preventing their collapse into IV clusters and sharpening the OOV boundary. As Fig. 6 (b) shows, IV samples form compact high-density clusters, while OOVs lie in the low-density gaps between them, modeling these gaps as priors guides pseudo-OOVs toward open space and enhances separability.

### 3.5. Total Loss

Our method can be trained end-to-end by minimizing the following loss function:

$$\mathcal{L} = \mathcal{L}_{align} + \mathcal{L}_{box} + \lambda \mathcal{L}_{LD-prior}, \quad (15)$$

where  $\mathcal{L}_{align}$  represents the similarity-based cross-entropy classification loss,  $\mathcal{L}_{box}$  represents the sum of the IoU loss and L1 regression loss of the prediction box.  $\lambda$  is the weighting coefficient of the OOV objective function  $\mathcal{L}_{LD-prior}$ .

Table 1. Zero-shot out-of-vocabulary object detection: comparisons on OOV-VOC and OOV-COCO. Best results are shown in **bold**, and second-best results are underlined. “ $\downarrow$ ” indicates that a smaller value is better, while “ $\uparrow$ ” indicates that a greater value is better.

OOV Datasets	Methods	mAP <sub>IV</sub> / mAP <sub>Oov</sub> $\uparrow$	mAP <sub>Seen</sub> / mAP <sub>Unseen</sub> $\uparrow$	Roov / ARoov $\uparrow$	WI / AOSE $\downarrow$
(a) OOV-VOC	Max Energy (Liu et al., 2020)	56.04 / 4.09	78.90 / 10.32	43.58 / 23.93	4.30 / 2381
	MSP (Sun et al., 2021)	55.51 / 5.50	78.34 / 9.84	<u>47.71</u> / 24.38	4.83 / 2651
	PROSER (Zhou et al., 2021)	55.63 / 5.99	78.55 / 9.79	35.85 / 18.26	4.94 / 2648
	OpenDet (Han et al., 2022)	55.44 / 2.43	77.61 / 2.43	46.61 / 23.77	4.42 / 2439
	GAIA (Chen et al., 2023)	52.23 / 4.86	73.13 / 10.36	45.56 / 23.65	4.82 / 2260
	EDL (Bao et al., 2021)	<u>57.90</u> / 2.02	<u>79.13</u> / 15.45	40.83 / 20.76	4.84 / 2702
	FOODv1 (Su et al., 2024)	57.56 / 1.20	79.05 / 13.39	42.38 / 18.62	4.31 / 2727
	FOODv2 (Su et al., 2023)	56.95 / 0.54	79.01 / 12.82	44.06 / 22.21	4.78 / 2641
	RegionCLIP (Zhong et al., 2022)	53.70 / 5.60	76.19 / 8.74	45.08 / 23.17	4.96 / 2567
	CoOp (Zhou et al., 2022a)	52.24 / <u>7.95</u>	76.55 / 3.64	47.43 / 23.47	4.64 / 2753
	CED-FOOD (Wu et al., 2025)	53.92 / 3.99	73.17 / 15.41	44.21 / 21.39	4.70 / <u>2228</u>
	APLGOS (Zhang et al., 2025)	42.62 / 3.39	73.02 / 10.82	47.53 / 23.84	4.80 / 2568
	<b>Our OOVDet</b>	<b>58.70/10.65</b>	<b>79.30/21.40</b>	<b>56.42/28.12</b>	<b>3.95/2142</b>
(b) OOV-COCO	Max Energy (Liu et al., 2020)	27.62 / 3.00	48.02 / 7.23	21.56 / 10.21	3.70 / <u>4278</u>
	MSP (Sun et al., 2021)	27.51 / 1.79	45.85 / 9.17	18.92 / 7.38	3.83 / 4773
	PROSER (Zhou et al., 2021)	27.88 / 2.86	46.03 / 9.72	18.30 / 7.27	3.85 / 4783
	OpenDet (Han et al., 2022)	27.54 / <u>5.24</u>	46.51 / 8.57	21.98 / 10.33	3.60 / 5228
	GAIA (Chen et al., 2023)	29.97 / 1.46	47.49 / 12.45	16.14 / 7.81	3.57 / 5148
	EDL (Bao et al., 2021)	26.59 / 5.22	47.17 / 6.00	20.45 / 9.60	3.61 / 4301
	FOODv1 (Su et al., 2024)	<u>32.63</u> / 4.01	<u>50.62</u> / 14.64	21.55 / 10.54	3.29 / 5194
	FOODv2 (Su et al., 2023)	32.03 / 3.59	50.04 / 13.67	22.14 / 10.93	<u>3.18</u> / 4878
	RegionCLIP (Zhong et al., 2022)	25.70 / 4.59	44.74 / 6.66	16.82 / 7.33	3.34 / 8252
	CoOp (Zhou et al., 2022a)	31.36 / 4.26	48.77 / <u>15.31</u>	<u>22.83</u> / <u>10.94</u>	3.95 / 5236
	CED-FOOD (Wu et al., 2025)	27.08 / 5.23	45.40 / 10.74	20.20 / 9.97	3.62 / 5596
	APLGOS (Zhang et al., 2025)	31.60 / 4.08	50.01 / 13.19	22.42 / 10.69	3.32 / 5421
	<b>Our OOVDet</b>	<b>33.19/10.09</b>	<b>51.15/15.89</b>	<b>27.60/12.82</b>	<b>3.12/4222</b>

## 4. Experiments

### 4.1. Experimental Detail

**Datasets.** We evaluate ZS-OOVD on six datasets. As illustrated in Fig. 3, OOV-VOC (Mark et al., 2010; Su et al., 2023; Wu et al., 2025) splits PASCAL VOC into 10 seen classes ( $C_{\text{Seen}}$ ), 5 unseen classes ( $C_{\text{Unseen}}$ ), and 5 OOV classes ( $C_{\text{OOV}}$ ). OOV-COCO (Lin et al., 2015; Su et al., 2023; Wu et al., 2025) further scales this setting to 20 VOC seen classes, 20 COCO unseen classes, and 40 COCO OOV classes for quantitative evaluation. In addition, we assess real-world generalization via qualitative OOV detection visualization on ObstacleTrack (Chan et al., 2021a), ADE-OoD (Galesso et al., 2024), MVTec-Anomaly (Bergmann et al., 2019), and RoadAnomaly (Lis et al., 2020).

**Evaluation Metrics.** The mean average precision (mAP) is chosen to evaluate the performance of IV classes, including mAP<sub>IV</sub>, mAP<sub>Oov</sub>, mAP<sub>Seen</sub>, and mAP<sub>Unseen</sub>. For the out-of-vocabulary evaluation, the recall (Roov) and average recall (ARoov) is reported. Furthermore, we report Wilderness Impact (WI) under a recall level of 0.8 to measure the degree of OOV objects misclassified to IV ones:  $WI = (\frac{P_{IV}}{P_{IV \cup OOV}} - 1) \times 100$ , where  $P_{IV}$  and  $P_{IV \cup OOV}$  denote the precision of close-set and open-set classes, respectively. Following (Han et al., 2022), we report WI under a recall level of 0.8. In addition, we also use the Absolute Open Set Error (AOSE) (Miller et al., 2018) to measure

the total number of OOV objects misclassified as IV.

**Implementation Details.** We build upon RegionCLIP using ResNet50, an ImageNet-pretrained offline RPN, and a CC3M-pretrained transformer text encoder (Zhong et al., 2022). Unlike CoOp-style methods (Zhou et al., 2022a), we freeze both the prompt learner and text encoder, and precompute IV text embeddings as fixed semantic prototypes, allowing the model to focus on visual–semantic alignment and OOV boundary modeling. Training is performed on four NVIDIA RTX 3090 GPUs with batch size 4, using SGD (base learning rate is  $5 \times 10^{-4}$ ), decayed once at 80k iterations, for 120k iterations without warm-up.

### 4.2. Main Results

**Experiments on OOV-VOC.** Table 1(a) shows that OOVDet outperforms state-of-the-art zero-shot OOV detectors on OOV-related metrics, achieving +2.70% mAP<sub>Oov</sub>, +8.71% Roov, +3.74% ARoov and reducing WI by 0.35 and AOSE by 86. This indicates stronger OOV recall with fewer IV false positives. OOVDet also maintains competitive IV performance, with mAP<sub>Unseen</sub>=21.40% (up 5.95% over EDL (Bao et al., 2021)) and mAP<sub>Seen</sub>=79.30%, demonstrating that OOV modeling does not compromise IV detection. Overall, OOVDet achieves a better balance between OOV sensitivity and IV stability.

**Experiments on OOV-COCO.** As shown in Table

**Table 2.** Ablation study of OOV prompt synthesis on OOV-VOC. We compare different prompt strategies and masking ratios under different backbones. Our ChatGPT-standardized Q&A prompts consistently outperform vanilla and handcrafted prompt variations in both IV and OOV metrics. Results demonstrate that class-conditional masked Gaussian perturbation  $\vec{\epsilon}$  effectively synthesizes informative OOV prompts, improving unseen-IV generalization and OOV rejection.

Prompt Strategy	Backbone + Text emb. dim	$\text{mAP}_{\text{IV}} / \text{mAP}_{\text{OOV}} \uparrow$	$\text{mAP}_{\text{Seen}} / \text{mAP}_{\text{Unseen}} \uparrow$	$\text{Roov} / \text{AR}_{\text{OOV}} \uparrow$	$\text{WI} / \text{AOSE} \downarrow$
“a region of a” + <cls>		58.21 / 3.58	78.74 / 17.16	54.13 / 26.98	4.44 / 2456
Common prompt variations (Zhong et al., 2022)	RN50+dim=1024	58.29 / 10.15	78.50 / 17.86	56.15 / 28.11	4.42 / 2450
ChatGPT standardized Q&A pairs (Ours)		<b>58.70 / 10.65</b>	<b>79.30 / 21.40</b>	<b>56.42 / 28.12</b>	<b>3.95 / 2142</b>
“a region of a” + <cls>		62.21 / 10.54	82.67 / 21.31	71.05 / 39.21	2.86 / 1669
Common prompt variations (Zhong et al., 2022)	RN50x4+dim=640	61.80 / 11.17	82.44 / 25.34	73.57 / 37.29	2.93 / 1761
ChatGPT standardized Q&A pairs (Ours)		<b>63.63 / 11.20</b>	<b>83.03 / 26.01</b>	<b>74.53 / 39.75</b>	<b>2.79 / 1695</b>
mask ratio=0.25		58.17 / 9.67	78.79 / 16.95	<b>70.66 / 35.07</b>	4.01 / 2487
<b>mask ratio=0.50</b>	RN50+dim=1024	<b>58.70 / 10.65</b>	<b>79.30 / 21.40</b>	56.42 / 28.12	<b>3.95 / 2142</b>
mask ratio=0.75		58.68 / 7.06	78.19 / 19.66	55.76 / 27.94	4.45 / 2406
mask ratio=1.00		58.14 / 5.58	78.52 / 21.38	44.75 / 23.18	4.39 / 2642

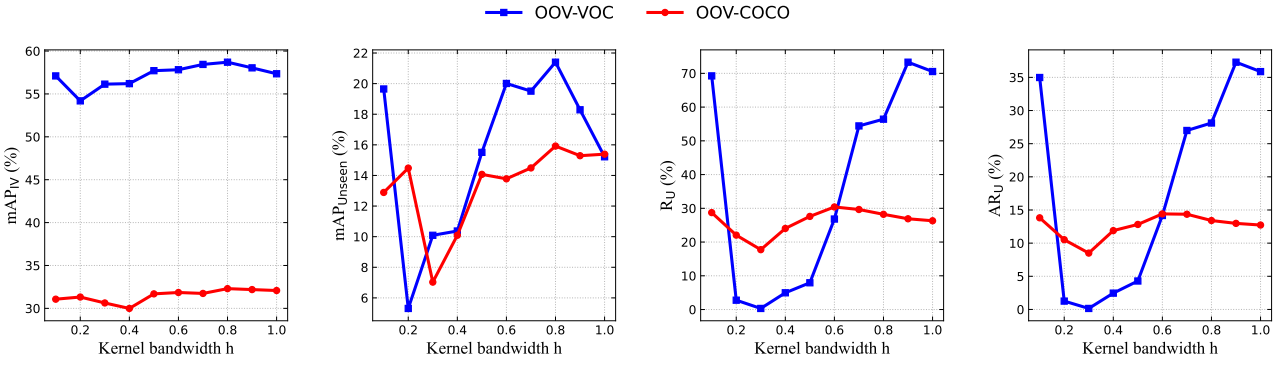


**Figure 4.** Effect of kernel bandwidth  $h$  on IV, unseen-IV, and OOV detection performance. We analyze the kernel bandwidth  $h$  in the Low-Density Prior Constraint on OOV-VOC and OOV-COCO, showing that  $h$  strongly affects both IV and OOV performance. A moderate bandwidth ( $h = 0.8$ ) provides the best trade-off, maximizing IV accuracy while preserving unseen-IV generalization and stable OOV detection. The blue and red lines correspond to OOV-VOC and OOV-COCO evaluations, respectively.

**Table 3.** Ablation study on pseudo-OOV image construction.

Top-k	fg:bg	$\text{mAP}_{\text{IV}} \uparrow$	$\text{mAP}_{\text{Unseen}} \uparrow$	$\text{R}_U \uparrow$	$\text{AR}_U \uparrow$
1	1:1	57.77	21.29	42.10	21.77
<b>3</b>	<b>1:1</b>	<b>58.70</b>	<b>21.40</b>	56.42	28.12
5	1:1	<u>58.64</u>	16.85	<b>71.70</b>	<b>36.11</b>
10	1:1	55.46	19.56	53.58	27.84
3	1:2	57.49	15.22	<u>71.44</u>	<u>36.06</u>
3	1:3	57.15	20.43	57.96	29.10

1(b), OOVDet achieves the best  $\text{mAP}_{\text{OOV}}=10.09\%$ , with  $\text{R}_{\text{OOV}}=27.60\%$  and  $\text{AR}_{\text{OOV}}=12.82\%$ , demonstrating strong localization and recall for diverse OOV instances. It also yields the lowest  $\text{WI}=3.12$  and  $\text{AOSE}=4222$ , indicating reduced IV-OOV confusion. Despite the increased difficulty, OOVDet maintains strong IV generalization ( $\text{mAP}_{\text{Seen}}=51.15\%$ ,  $\text{mAP}_{\text{Unseen}}=15.89\%$ ), confirming its scalability to large OOV spaces.

### 4.3. Ablation Study

**Ablation on OOV Prompt Synthesis.** Table 2 shows that under RN50, our ChatGPT-standardized Q&A prompts achieve 58.70%  $\text{mAP}_{\text{IV}}$  and 21.40%  $\text{mAP}_{\text{Unseen}}$ , improving  $\text{AR}_{\text{OOV}}$  (26.98%  $\rightarrow$  28.12%) and reducing  $\text{WI}$  (4.44  $\rightarrow$  3.95) compared to the vanilla template. Similar gains are observed with RN50x4 (63.63% / 26.01%), indicating good robustness across backbones. A mask ratio of 0.50 yields the best trade-off, validating that our prompt synthesis with moderate perturbation effectively generates informative OOV prompts in low-density regions.

**Ablation on Pseudo-OOV Image.** Table 3 shows that increasing Top- $k$  from 1 to 3 improves  $\text{mAP}_{\text{IV}}$  (57.77%  $\rightarrow$  58.70%),  $\text{mAP}_{\text{Unseen}}$  (21.29%  $\rightarrow$  21.40%) and OOV recall  $R_U$  (42.10%  $\rightarrow$  56.42%), while larger Top- $k$  (5 or 10) increases recall but degrades unseen performance due to noisy gradients. Increasing background proportion also boosts  $R_U$  but harms  $\text{mAP}_{\text{Unseen}}$ . The best balance is achieved at Top- $k = 3$  and fg:bg=1:1, validating DGA’s effectiveness.

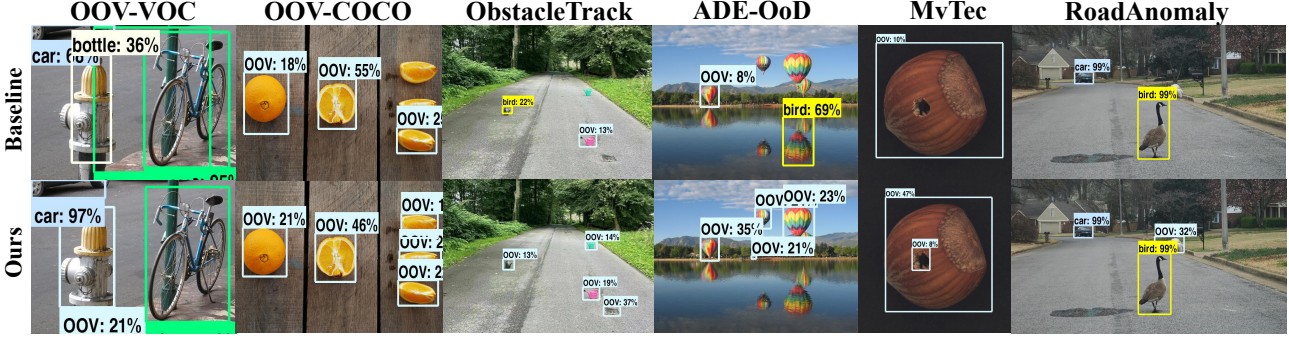


Figure 5. The visualized results on OOV-VOC, OOV-COCO and diverse real-world datasets.

Table 4. Effect of kernel bandwidth  $h$  on OOV-VOC.

$h$	$mAP_{IV}\uparrow$	$mAP_{Unseen}\uparrow$	$R_U\uparrow$	$AR_U\uparrow$
0.1	57.10	19.65	69.25	34.98
0.2	54.19	5.31	2.77	1.26
0.3	56.14	10.09	0.32	0.15
0.4	56.20	10.37	4.96	2.46
0.5	57.71	15.51	7.93	4.29
0.6	57.82	20.01	26.82	14.17
0.7	<u>58.44</u>	19.51	54.42	26.99
<b>0.8</b>	<b>58.70</b>	<b>21.40</b>	56.42	28.12
0.9	58.04	18.29	<b>73.31</b>	<b>37.29</b>
1.0	57.35	15.22	<u>70.54</u>	<u>35.87</u>

**Ablation on OOV Optimization.** Fig. 4 shows that the kernel bandwidth  $h$  critically controls the Low-Density Prior Constraint. On OOV-VOC (Table 4),  $h = 0.8$  achieves the best  $mAP_{IV}$  (58.70%) while maintaining strong unseen-IV generalization ( $mAP_{Unseen}=21.40\%$ ) and competitive OOV detection ( $AR_U=28.12\%$ ). A similar trend holds on OOV-COCO, where too small  $h$  destabilizes density estimation and too large  $h$  over-smooths it. Thus,  $h = 0.8$  is adopted in all experiments.

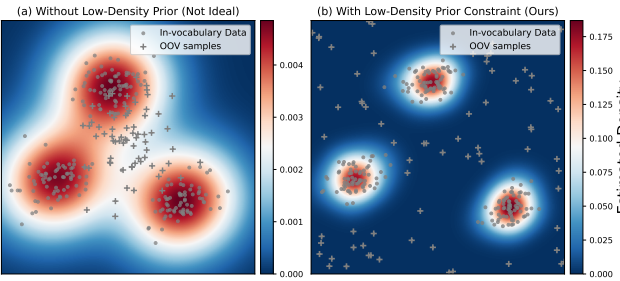


Figure 6. Visualization of the proposed Low-Density Prior Constraint in the feature space.

**Effect of the Low-Density Prior Constraint.** Fig. 6 visualizes the Low-Density Prior Constraint. Without it, IV density is diffuse and OOV samples (gray “+”) lie near IV

clusters, causing entangled decision regions. With the constraint, IV features form compact high-density modes and OOV samples are pushed into low-density valleys, yielding clearer boundaries. This aligns with our design, where high-uncertainty OOV-related samples in high IV density regions are penalized, improving IV compactness, unseen-IV generalization, and OOV rejection.

#### 4.4. Visualization of OOV Detection Results

Fig. ?? shows that on OOV-VOC and OOV-COCO, the baseline often misclassifies OOV objects as semantically similar IV categories with high confidence, whereas our method assigns higher OOV confidence and suppresses incorrect IV predictions, yielding clearer IV-OOV separation. On more complex benchmarks with severe domain shifts and complex visual patterns, including ObstacleTrack, ADE-OoD, MVtec Anomaly, and RoadAnomaly, the baseline frequently produces unstable, erroneous high-confidence IV detections on OOV regions. In contrast, our approach remains robust by reliably identifying unknown and anomalous regions as OOV while maintaining stable IV detection, reflecting more trustworthy prediction confidence in open-world scenarios. Additional visualizations and ablations are provided in Appendix.

## 5. Conclusion

This paper studies zero-shot out-of-vocabulary detection (ZS-OOVD), an underexplored yet critical problem in open-world object detection, which requires reliable in-vocabulary recognition while rejecting undefined objects without training samples or semantic prompts. We propose OOVDet, a unified framework integrating OPS, DGA, and LPC to explicitly model the discrepancy between in-vocabulary and out-of-vocabulary samples, enabling robust IV-OOV discrimination. Extensive experiments across multiple benchmarks validate the effectiveness of the proposed approach. Overall, this work takes a practical step toward reliable open-world object detection under zero-shot constraints and highlights the importance of OOV-aware representation and decision boundary modeling.

## References

Bansal, A., Sikka, K., Sharma, G., Chellappa, R., and Divakaran, A. Zero-shot object detection. In *Proceedings of the European Conference on Computer Vision (ECCV)*, pp. 384–400, September 2018.

Bao, W., Yu, Q., and Kong, Y. Evidential deep learning for open set action recognition. In *Proceedings of the IEEE/CVF International Conference on Computer Vision (ICCV)*, pp. 13349–13358, October 2021.

Bergmann, P., Fauser, M., Sattlegger, D., and Steger, C. Mvtec ad — a comprehensive real-world dataset for unsupervised anomaly detection. In *2019 IEEE/CVF Conference on Computer Vision and Pattern Recognition (CVPR)*, pp. 9584–9592, 2019.

Chan, R., Lis, K., Uhlemeyer, S., Blum, H., Honari, S., Siegwart, R., Fua, P., Salzmann, M., and Rottmann, M. Segmentmeifyoucan: A benchmark for anomaly segmentation. *Thirty-fifth Conference on Neural Information Processing Systems*, 2021a.

Chan, R., Rottmann, M., and Gottschalk, H. Entropy maximization and meta classification for out-of-distribution detection in semantic segmentation. In *Proceedings of the IEEE/CVF International Conference on Computer Vision (ICCV)*, pp. 5128–5137, October 2021b.

Chen, J., Li, J., Qu, X., Wang, J., Wan, J., and Xiao, J. Gaia: Delving into gradient-based attribution abnormality for out-of-distribution detection. In Oh, A., Naumann, T., Globerson, A., Saenko, K., Hardt, M., and Levine, S. (eds.), *Advances in Neural Information Processing Systems*, volume 36, pp. 79946–79958. Curran Associates, Inc., 2023.

Cheng, T., Song, L., Ge, Y., Liu, W., Wang, X., and Shan, Y. Yolo-world: Real-time open-vocabulary object detection. In *Proceedings of the IEEE/CVF Conference on Computer Vision and Pattern Recognition (CVPR)*, pp. 16901–16911, June 2024.

Du, X., Wang, Z., Cai, M., and Li, Y. Vos: Learning what you don't know by virtual outlier synthesis. In *Proc. Int. Conf. Learn. Represent. (ICLR)*, 2022.

Du, X., Sun, Y., Zhu, J., and Li, Y. Dream the impossible: Outlier imagination with diffusion models. In Oh, A., Naumann, T., Globerson, A., Saenko, K., Hardt, M., and Levine, S. (eds.), *Advances in Neural Information Processing Systems*, volume 36, pp. 60878–60901. Curran Associates, Inc., 2023.

Galessos, S., Schröppel, P., Driss, H., and Brox, T. Diffusion for out-of-distribution detection on road scenes and beyond. In *ECCV*, 2024.

Guo, W., Du, Y., and Du, S. Langgas: Introducing language in selective zero-shot background subtraction for semi-transparent gas leak detection with a new dataset. In *Proceedings of the IEEE/CVF Conference on Computer Vision and Pattern Recognition (CVPR) Workshops*, pp. 4499–4509, June 2025.

Han, J., Ren, Y., Ding, J., Pan, X., Yan, K., and Xia, G. Expanding low-density latent regions for open-set object detection. In *Proceedings of the IEEE/CVF Conference on Computer Vision and Pattern Recognition (CVPR)*, 2022.

Holub, A., Perona, P., and Burl, M. C. Entropy-based active learning for object recognition. In *2008 IEEE Computer Society Conference on Computer Vision and Pattern Recognition Workshops*, pp. 1–8, 2008. doi: 10.1109/CVPRW.2008.4563068.

Jeong, M., Choi, S., and Kim, C. Few-shot open-set recognition by transformation consistency. In *Proceedings of the IEEE/CVF Conference on Computer Vision and Pattern Recognition (CVPR)*, pp. 12566–12575, June 2021.

Joseph, K. J., Khan, S., Khan, F. S., and Balasubramanian, V. N. Towards open world object detection. In *Proceedings of the IEEE/CVF Conference on Computer Vision and Pattern Recognition (CVPR)*, pp. 5830–5840, June 2021.

Li, H. and Zhang, T. Outlier synthesis via hamiltonian monte carlo for out-of-distribution detection. In *The Thirteenth International Conference on Learning Representations*.

Li, J. and Dong, Q. Open-set semantic segmentation for point clouds via adversarial prototype framework. In *Proceedings of the IEEE/CVF Conference on Computer Vision and Pattern Recognition (CVPR)*, pp. 9425–9434, June 2023.

Lin, T.-Y., Maire, M., Belongie, S., Bourdev, L., Girshick, R., Hays, J., Perona, P., Ramanan, D., Zitnick, C. L., and Dollár, P. Microsoft coco: Common objects in context. In *Proc. Eur. Conf. Comput. Vis. (ECCV)*, 2015.

Lis, K., Nitsch, J., Blume, H., Widder, P., Holz, P., Bleyer, M., and Schindler, K. Detecting unexpected obstacles for self-driving cars: Fusing deep learning and geometric modeling. In *Proceedings of the IEEE/CVF International Conference on Robotics and Automation (ICRA)*, pp. 208–214, 2020.

Liu, W., Wang, X., Owens, J., and Li, Y. Energy-based out-of-distribution detection. In Larochelle, H., Ranzato, M., Hadsell, R., Balcan, M., and Lin, H. (eds.), *Advances in Neural Information Processing Systems*, volume 33, pp. 21464–21475. Curran Associates, Inc., 2020.

Mark, E., Luc, V., and Christopher, W. The pascal visual object classes (voc) challenge. In *Proc. IEEE Int. Conf. Comput. Vis. (ICCV)*, 2010.

Miller, D., Nicholson, L., Dayoub, F., and Sünderhauf, N. Dropout sampling for robust object detection in open-set conditions. In *2018 IEEE International Conference on Robotics and Automation (ICRA)*, pp. 3243–3249, 2018. doi: 10.1109/ICRA.2018.8460700.

Minderer, M., Gritsenko, A., and Stone, A. Simple open-vocabulary object detection. In *Proceedings of the European Conference on Computer Vision (ECCV)*, pp. 728–755, 2022.

Minderer, M., Gritsenko, A., and Houlsby, N. Scaling open-vocabulary object detection. In Oh, A., Naumann, T., Globerson, A., Saenko, K., Hardt, M., and Levine, S. (eds.), *Advances in Neural Information Processing Systems*, volume 36, pp. 72983–73007. Curran Associates, Inc., 2023.

Qutub, S. S., Paulitsch, M., Scholl, K.-U., Cihangir, N. K., Hagn, K., Oboril, F., Hinz, G., and Knoll, A. Situation monitor: Diversity-driven zero-shot out-of-distribution detection using budding ensemble architecture for object detection. In *Proceedings of the IEEE/CVF Conference on Computer Vision and Pattern Recognition (CVPR) Workshops*, pp. 3502–3511, June 2024.

Radford, A., Kim, J. W., Hallacy, C., Ramesh, A., Goh, G., Agarwal, S., Sastry, G., Askell, A., Mishkin, P., Clark, J., Krueger, G., and Sutskever, I. Learning transferable visual models from natural language supervision. In Meila, M. and Zhang, T. (eds.), *Proceedings of the 38th International Conference on Machine Learning*, volume 139 of *Proceedings of Machine Learning Research*, pp. 8748–8763, 18–24 Jul 2021.

Ren, M., Triantafillou, E., Ravi, S., Snell, J., Swersky, K., Tenenbaum, J. B., Larochelle, H., and Zemel, R. S. Meta-learning for semi-supervised few-shot classification. *arXiv preprint arXiv:1803.00676*, 2018.

Sarkar, H., Chudasama, V., Onoe, N., Wasnik, P., and Balasubramanian, V. N. Open-set object detection by aligning known class representations. In *Proceedings of the IEEE/CVF Winter Conference on Applications of Computer Vision (WACV)*, pp. 219–228, January 2024.

Selvaraju, R. R., Cogswell, M., Das, A., Vedantam, R., Parikh, D., and Batra, D. Grad-cam: Visual explanations from deep networks via gradient-based localization. In *2017 IEEE International Conference on Computer Vision (ICCV)*, pp. 618–626, 2017. doi: 10.1109/ICCV.2017.74.

Sensoy, M., Kaplan, L., and Kandemir, M. Evidential deep learning to quantify classification uncertainty. In Bengio, S., Wallach, H., Larochelle, H., Grauman, K., Cesa-Bianchi, N., and Garnett, R. (eds.), *Advances in Neural Information Processing Systems*, volume 31. Curran Associates, Inc., 2018.

Simonyan, K., Vedaldi, A., and Zisserman, A. Deep inside convolutional networks: Visualising image classification models and saliency maps. *International Conference on Learning Representations*, 2013.

Su, B., Zhang, H., and Zhou, Z. Hsic-based moving weight averaging for few-shot open-set object detection. In *Proceedings of the 31st ACM International Conference on Multimedia (MM 23)*, 2023. doi: <https://doi.org/10.1145/3581783.3611850>.

Su, B., Zhang, H., Li, J., and Zhou, Z. Toward generalized few-shot open-set object detection. *IEEE Transactions on Image Processing*, 33:1389–1402, 2024. doi: 10.1109/TIP.2024.3364495.

Sun, Y., Guo, C., and Li, Y. React: Out-of-distribution detection with rectified activations. In Ranzato, M., Beygelzimer, A., Dauphin, Y., Liang, P., and Vaughan, J. W. (eds.), *Advances in Neural Information Processing Systems*, volume 34, pp. 144–157. Curran Associates, Inc., 2021.

Wang, R., Zhao, R.-W., Zhang, X., and Feng, R. Towards evidential and class separable open set object detection. *Proceedings of the AAAI Conference on Artificial Intelligence*, 38(6):5572–5580, Mar. 2024. doi: 10.1109/aaai.v38i6.28367.

Wu, Z., Su, B., Geng, Q., Zhang, H., and Zhou, Z. Boosting few-shot open-set object detection via prompt learning and robust decision boundary. In *Proceedings of the Thirty-Fourth International Joint Conference on Artificial Intelligence (IJCAI)*, pp. 6606–6614, 2025.

Young, S. Detecting misrecognition and out-of-vocabulary words. In *Proceedings of ICASSP '94. IEEE International Conference on Acoustics, Speech and Signal Processing*, volume ii, pp. II/21–II/24 vol.2, 1994. doi: 10.1109/ICASSP.1994.389728.

Zhang, Q., Li, X., Lu, J., Qiu, L., Pan, S., Chen, X., and Chen, J. Rog-pl: Robust open-set graph learning via region-based prototype learning. In *Proceedings of the AAAI Conference on Artificial Intelligence*, pp. 9350–9358, Mar 2024.

Zhang, Y., She, D., and Zhou, Z. Adaptive prompt learning via gaussian outlier synthesis for out-of-distribution detection. In *Proceedings of the IEEE/CVF International Conference on Computer Vision*, pp. 3235–3244, 2025.

Zhong, Y., Yang, J., Zhang, P., Li, C., Codella, N., Li, L. H., Zhou, L., Dai, X., Yuan, L., Li, Y., and Gao, J. Regionclip: Region-based language-image pretraining. In *Proceedings of the IEEE/CVF Conference on Computer Vision and Pattern Recognition (CVPR)*, pp. 16793–16803, June 2022.

Zhou, D.-W., Ye, H.-J., and Zhan, D.-C. Learning place-holders for open-set recognition. In *Proceedings of the IEEE/CVF conference on computer vision and pattern recognition*, pp. 4401–4410, 2021.

Zhou, K., Yang, J., Loy, C. C., and Liu, Z. Learning to prompt for vision-language models. *International Journal of Computer Vision*, 130(9):2337–2348, 2022a.

Zhou, K., Yang, J., Loy, C. C., and Liu, Z. Learning to prompt for vision-language models. *International Journal of Computer Vision*, 130(9):2337–2348, 2022b.

## A. Related Works

**Open-Set Object Detection** Open-set object detection (OSOD) aims to detect all known classes at inference while rejecting undefined categories as unknowns, thereby preventing unknown objects from being misclassified as known ones with high confidence. According to the identification way of the unknown samples, OSOD can be mainly divided into four categories. 1) Prototype-based methods. This type of methods measures the distance between the query input and known class prototypes to recognize the open-set classes, such as SnaTCHer (Jeong et al., 2021), APF (Li & Dong, 2023), and ROG (Zhang et al., 2024). 2) Generation-based approaches. This line of works synthesizes the virtual unknown samples to regularize the model’s decision boundary, such as VOS (Du et al., 2022) and Dream-OOD (Du et al., 2023). 3) Threshold-based approaches. This form of works uses energy (Liu et al., 2020; Joseph et al., 2021), entropy (Holub et al., 2008; Chan et al., 2021b), evidence (Bao et al., 2021; Wang et al., 2024) etc. as an open-set score, which is compared with a threshold to reject unknown classes. 4) Uncertainty-based methods. This kind of works estimates the uncertainty of the input query, where the higher the uncertainty, the greater the probability of the unknown class, such as OpenDet (Han et al., 2022) and FOOD (Su et al., 2023). Drawing lessons from uncertainty-based methods, we explore the Dirichlet-based gradient attribution method for uncertainty estimation, then mine high-uncertainty samples for unknown optimization.

**Pseudo-Sample Mining** Since no training samples exist for unknown classes, the goal of pseudo-sample mining is to identify highly uncertain samples from both foreground and background regions, which are then used to optimize the representation of unknown classes. FOODv1 (Su et al., 2024) and FOODv2 (Su et al., 2023) employ conditional energy and evidential learning (Sensoy et al., 2018; Bao et al., 2021) to estimate the uncertainty of region proposals, respectively, for pseudo-sample mining. HamOS (Li & Zhang) synthesizes pseudo-unknowns via Hamiltonian Monte Carlo for out-of-distribution detection. Referring to GradCAM (Selvaraju et al., 2017), GAIA (Chen et al., 2023) directly uses gradient to attribute the uncertainty of input image. Drawing inspiration from the gradient-based attribution methods and evidential learning for uncertainty estimation, we propose a Dirichlet-based gradient attribution (DGA) method to select pseudo-OOV images from both foreground and background regions, and further achieves superior performance.

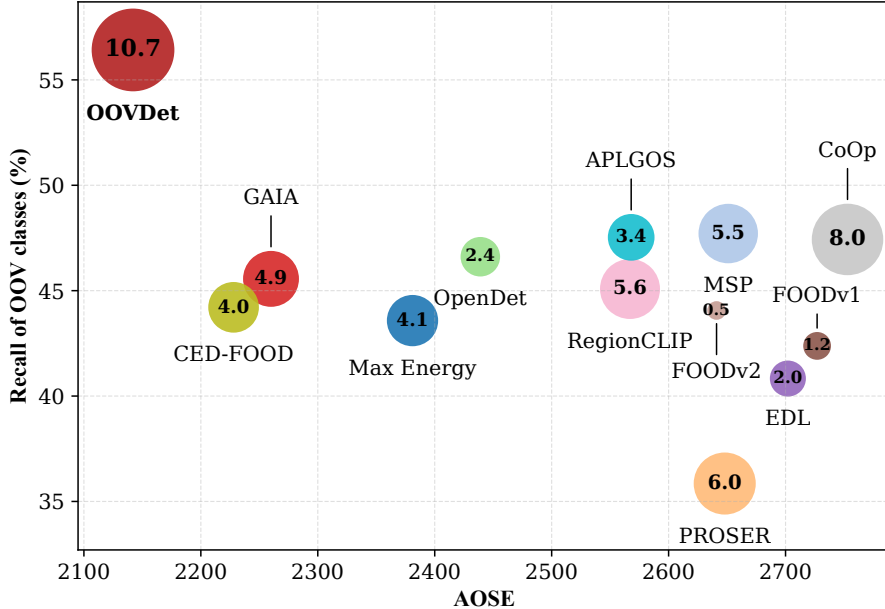


Figure 7. Trade-off between out-of-vocabulary recall and open-set error in the OOV-VOC dataset.

## B. Comparison of Our Method with Other Approaches

We compare the vision-only open-set methods such as Max Energy (Liu et al., 2020), MSP (Sun et al., 2021), PROSER (Zhou et al., 2021), OpenDet (Han et al., 2022), GAIA (Chen et al., 2023), EDL (Bao et al., 2021), FOODv1 (Su et al., 2024), and FOODv2 (Su et al., 2023). For a fair comparison, building upon RegionCLIP, we primarily leverage the pseudo-image mining algorithms from the aforementioned methods to extract high-uncertainty pseudo-OOV images, while simultaneously adopting the OOV decoupling optimization (Han et al., 2022) to construct the OOV decision boundary. Furthermore, we

compare several vision-language-based methods, such as RegionCLIP (Zhong et al., 2022), CoOp (Zhou et al., 2022a), CED-FOOD (Wu et al., 2025), and APLGOS (Zhang et al., 2025), which are modified as ZS-OOVD algorithms. For RegionCLIP and APLGOS, we preserve a placeholder for the OOV class, and employ an EDL-based uncertainty estimation method to mine pseudo-OOV images for optimization. For CoOp, we introduce learnable context prompts to jointly model both IV and OOV classes. CED-FOOD is a few-shot open-set object detection method, in which we employ attribution gradients to mine high-uncertainty samples for OOV optimization. Meanwhile, the Conditional Evidential Decoupling mechanism proposed in CED-FOOD is adopted to construct the OOV decision boundary for the above vision-language-based methods.

The figure compares different ZS-OOVD methods in terms of **Roov** (higher is better) and **AOSE** (lower is better). Each bubble represents a method, where the bubble size is proportional to **mAP<sub>OOV</sub>**. The proposed OOVDet achieves a superior trade-off, simultaneously yielding the lowest **AOSE** and the highest **Roov** among all competitors. Leader lines are used to avoid label overlap for clarity. As evidenced in Fig. 7, our OOVDet substantially outperforms prior state-of-the-art approaches across all out-of-vocabulary metrics.

### C. Additional Visualization Results

As shown in Fig. 8, we provide qualitative comparisons between a representative baseline and the proposed OOVDet on OOV-VOC and OOV-COCO. The baseline method frequently misclassifies out-of-vocabulary objects as in-vocabulary categories with high confidence, indicating severe overfitting to the predefined vocabulary and poor unknown rejection capability. In contrast, OOVDet consistently assigns higher OOV confidence scores to unknown objects while effectively suppressing erroneous in-vocabulary predictions, even in cluttered scenes containing both IV and OOV instances. Notably, this behavior is consistently observed across both OOV-VOC and the more challenging OOV-COCO benchmark, demonstrating the robustness and scalability of the proposed approach under expanded OOV category spaces.

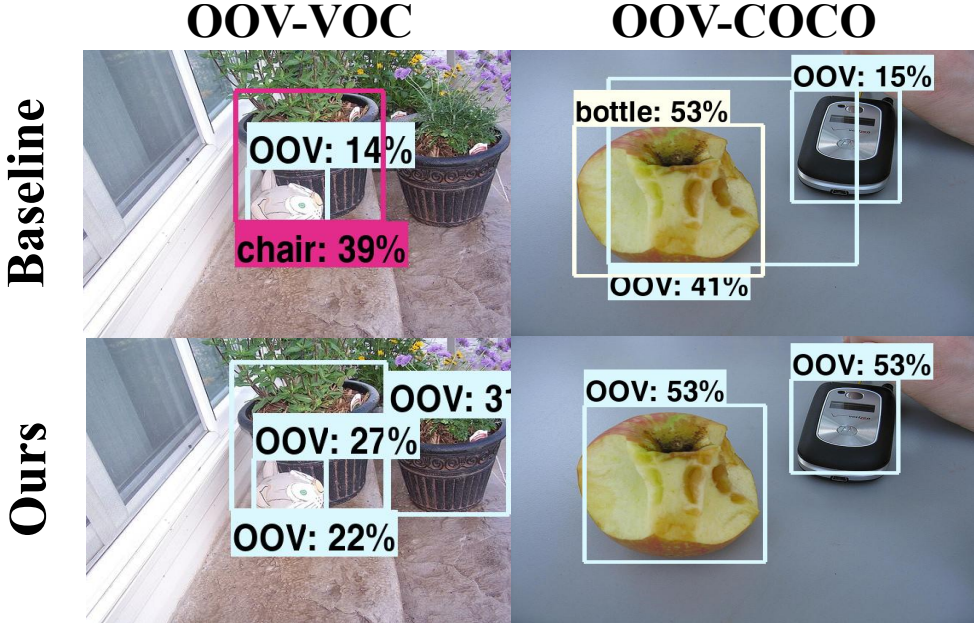


Figure 8. Qualitative visualization of zero-shot out-of-vocabulary detection results on OOV-VOC and OOV-COCO.

As illustrated in Fig. 9, qualitative results are reported on **ObstacleTrack**, **ADE-OoD**, **MVTec Anomaly**, and **RoadAnomaly** from top to bottom, spanning road scenes, natural environments, industrial inspection, and anomaly-dominated open-world scenarios. Bounding boxes indicate detected regions, while the associated **OOV confidence scores** reflect the model’s estimation of out-of-vocabulary likelihood. Notably, these datasets exhibit severe domain shifts, substantial appearance diversity, and semantic distributions that are largely disjoint from the training vocabulary, with no access to training images or prompts for OOV categories. Despite these challenges, the proposed method consistently localizes OOV and anomalous objects with high confidence across all scenarios, providing compelling qualitative evidence of its robustness, semantic generalization ability, and practical effectiveness for realistic open-world perception.

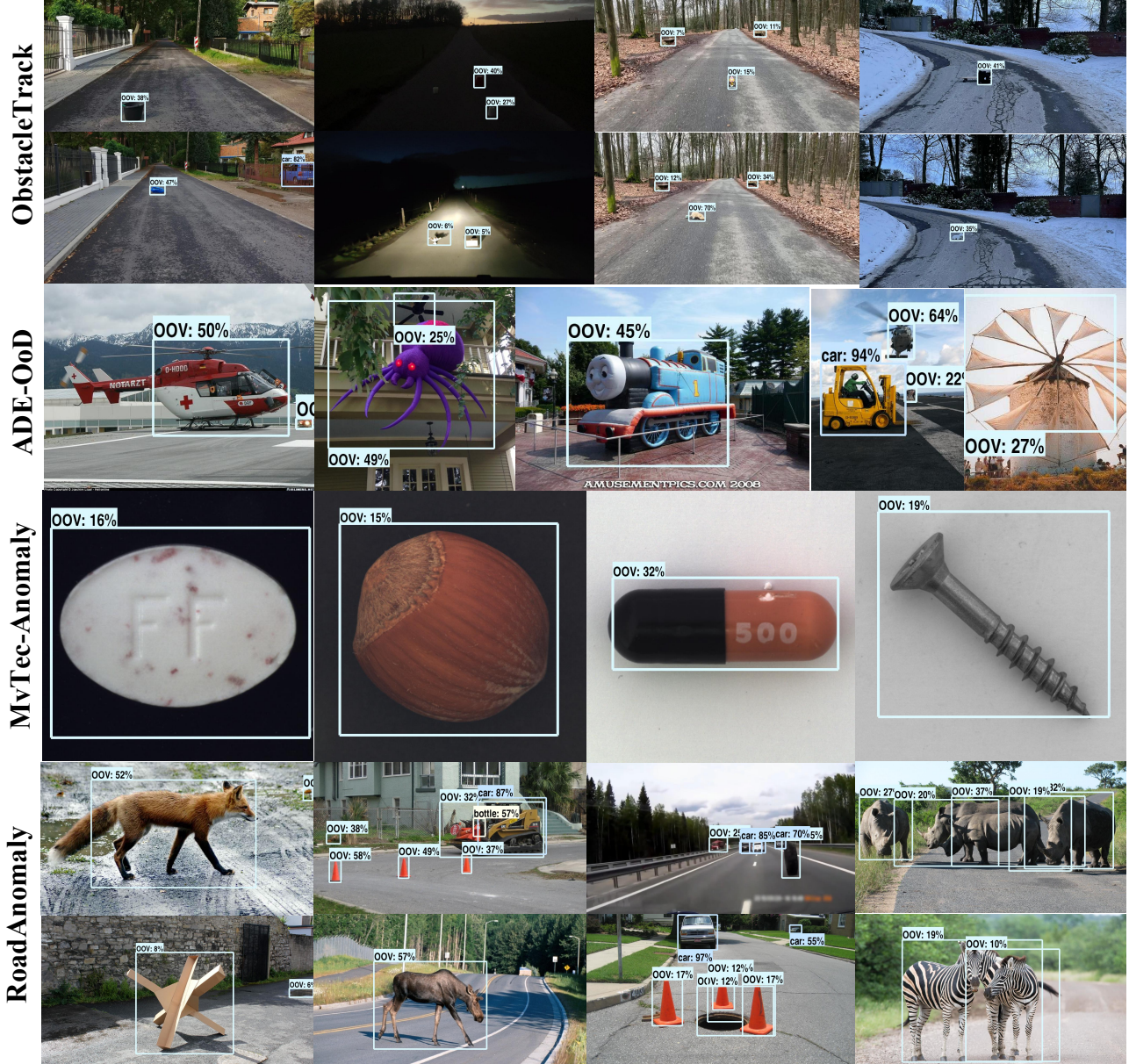


Figure 9. Qualitative visualization of zero-shot out-of-vocabulary detection results on diverse real-world datasets.